

# Performance and mechanism of the separation of C8 $\alpha$ -olefin from F-T synthesis products using novel Ag-DES

Hu Li<sup>1</sup> | Zisheng Zhang<sup>1,3</sup> | Guanlun Sun<sup>1</sup> | Suli Liu<sup>2</sup> | Liangcheng An<sup>2</sup> |

Xingang Li<sup>1</sup> | Hong Li<sup>1</sup> | Xin Gao<sup>1,\*</sup>

<sup>1</sup>School of Chemical Engineering and Technology, National Engineering Research Center of Distillation Technology, Collaborative Innovation Center of Chemical Science and Engineering (Tianjin), Tianjin University, Tianjin 300072, China

<sup>2</sup>Ningxia Coal Industry Group Co. Ltd., CHN ENERGY, Yinchuan 750011, PR China

<sup>3</sup>Department of Chemical and Biological Engineering, University of Ottawa, Ottawa K1N 6N5, Canada

## Corresponding author

Xin Gao, School of Chemical Engineering and Technology, National Engineering Research Center of Distillation Technology, Collaborative Innovation Center of Chemical Science and Engineering (Tianjin), Tianjin University, Tianjin 300072, China.

Email: gaoxin@tju.edu.cn

## Funding information

National Key R&D Program of China, Grant/Award Numbers: 2018YFB0604900; Key Research and Development program of Ningxia, Grant/Award Numbers: 2018BDE02057

**Abstract:** As an attractive alternative technology for the separation of long chain olefin and paraffin, a novel silver-based deep eutectic solvent (Ag-DES) was prepared and utilized for 1-octene/n-octane separations. Comprehensive reactive extraction separation experiments were performed to highlight the Ag-DES concentration and operating temperature discriminations using compounds with different ratio of 1-octene/n-octane. The novel Ag-

DES showed optimal separation performance regarding 1-octene/n-octane and possessed the highest levels separation selectivity in the range 3.75-16.74 with excellent circulation stability in our best knowledge. Furthermore, FT-Raman measurements and quantum chemistry calculation were performed to elucidate the interaction mechanism of Ag-DES in the separation of 1-octene and n-octane, which revealed that both chemical complexation and strong physical attraction existed in the complex of Ag-DES with 1-octene rather than n-octane. This study lends important insight for the development of Ag-DES reactive extraction separation process for the energy-efficient long chain  $\alpha$ -olefin purification from F-T synthesis products.

## KEYWORDS

silver-based deep eutectic solvent, reactive extraction, separation, 1-octene,  $\alpha$ -olefin

## 1 | INTRODUCTION

Long chain  $\alpha$ -olefins have extremely high added-value, which are widely used as comonomers for polymers such as polyethylene, the synthesis of halogenated hydrocarbons, and oligomerization to lubricating oils, etc.<sup>1</sup> At present, the production of long chain  $\alpha$ -olefins in industry is mainly obtained from ethylene oligomerization and separation from Fischer-Tropsch stream.<sup>2,3</sup> Although the former process is simple, the heavy byproducts are serious and cost much more money.<sup>4</sup> The liquid products of Fischer-Tropsch synthesis are valuable raw materials for the separation of long chain  $\alpha$ -olefins because of the relatively higher content of  $\alpha$ -olefins with carbon number of 6–25,<sup>5</sup> whereas they are used as low-value fuels at present. The  $\alpha$ -olefins separated from Fischer-Tropsch synthesis products are a commercially valuable class of chemical compounds. However, the separation process is currently one of

the most energy-intensive and costly processes in the petrochemical industry, because of the structural similarity and lower relative volatility between olefins and paraffins with the same carbon number.

A series of researches were focused on the purification of  $\alpha$ -olefins from olefin/paraffin mixtures including with 1-octene/n-octane. Distillation method is an energy- and capital-intensive scheme required a plurality of columns, a large number distillation trays and higher reflux ratio.<sup>6</sup> Physical and chemical adsorption were rarely employed to separate liquid  $\alpha$ -olefins with the difficulty in determination of adsorption capacity.<sup>1,7</sup> Facilitated transport membrane containing transition metal has been widely studied and applied in the separation of olefin/paraffin recent years, especially silver ion and cuprous ion.<sup>8,9</sup> The chemical complexation between the transition metal cations and the double bond of olefin can effectively achieve the selective separation of  $\alpha$ -olefins.<sup>10</sup> Liu et al.<sup>11</sup> and Rychlewska et al.<sup>12</sup> obtained extremely high permeability and separation selectivity in the separation of 1-hexene/n-hexane and 1-octene/n-octane mixtures due to the dissolution and diffusion differences on the facilitated transport membrane. However, it is limited to large-scale application because of low transported capacity and high cost.<sup>13</sup> Considering the above processes with various problems, it is of great necessity to develop an alternative technology with a good selectivity for  $\alpha$ -olefins, eco-efficiency, stable physicochemical properties, easy recovery and pollution-free. As a green designable solvent, deep eutectic solvents (DESs) and ionic liquids (ILs) have these characteristics.<sup>14,15</sup> Among them, transition metal-based deep eutectic solvent is a more promising reactive extractant for the separation of  $\alpha$ -olefins with great application potential.

A deep eutectic solvent is a fluid mixture composed of two or more safe components through hydrogen bonds with lower melting point than any of their individual component.<sup>16,17</sup> Compared with the traditional solvent ILs, most of DESs exhibit a lot of remarkable advantages such as desirable biodegradability, environmental friendliness, ease of preparation for large-scale applications and show great interests in many fields.<sup>16,18</sup> DESs have been widely used in the extraction separations,<sup>18</sup> natural products extraction,<sup>19</sup> gaseous mixture separations,<sup>20,21</sup> catalysis,<sup>22,23</sup> dissolution and modification processes,<sup>24</sup> electrochemistry<sup>25</sup> and material chemistry.<sup>26</sup> Jiang et al.<sup>27,28</sup> have achieved a good separation selectivity in the separation of ethylene/ethane with DESs as supported liquid membranes. However, there are almost no researches to report the application of DESs in the separation of liquid  $\alpha$ -olefins, such as 1-hexene/n-hexane and 1-octene/n-octane. Nevertheless, the olefin-to-paraffin selectivity in pure ILs and DESs without transition metal is very low.<sup>13,14</sup> Considering the chemical complexation between the transition metal cations and double bond of olefin, the addition of silver-based cation can greatly improve the olefin selectivity and separation efficiency. Therefore, to design and prepare silver-based DESs to enhance olefin-to-paraffin selectivity is of great necessity. The study of interaction mechanism is favorable to optimizing the extractant structure and further improving the separation performance.

Based on these reasons, we designed and prepared a novel sustainable silver-based deep eutectic solvent (Ag-DES) consisted of N,N-dimethylbenzamide (DMBA) and silver trifluoromethanesulfonate ( $\text{AgCF}_3\text{SO}_3$ ). The structure of Ag-DES was characterized by FT-IR, FT-Raman,  $^1\text{H}$  NMR, and ESI-MS. The effect of olefin concentration, molar ratio of Ag-DES to 1-octene, operating temperature on the distribution coefficient and the selectivity of

olefin to paraffin were investigated in the binary 1-octene/n-octane mixture. The long-term stability of the Ag-DES was evaluated by repeated circulation stability experiments. In addition, quantum chemistry calculation was carried out by using Gaussian 09 software package based on density functional theory (DFT) to calculate the optimized geometries, interaction energies, combined the measurements results from FT-Raman to analyze the intermolecular covalent and non-covalent interactions and reveal the interaction mechanism of Ag-DES with 1-octene and n-octane. In particular, this study will provide a novel insight for the role of Ag-DES for separation of the long chain olefins/paraffin, which is of great help for us to screen new Ag-DES for separation of  $\alpha$ -olefins from F-T synthesis products.

## **2 | EXPERIMENTAL SECTION**

### **2.1 | Materials and reagents**

1-octene (> 98 wt.%) was purchased from Shanghai Maclean Biochemical Technology Co., Ltd. (Shanghai, China). n-octane (> 99 wt.%) was purchased from Tianjin Jiangtian Chemical Technology Co., Ltd. (Tianjin, China). N,N-dimethylbenzamide (DMBA, > 99.9 wt.%) was provided by Shanghai Aladdin Biochemical Technology Co., Ltd. (Shanghai, China). Silver trifluoromethanesulfonate ( $\text{AgCF}_3\text{SO}_3$ ,  $\geq 99.8$  wt.%) was supplied by Shanghai Haohong Biomedical Technology Co., Ltd. (Shanghai, China). All chemicals were used as received without further purification.

### **2.2 | Preparation of Ag-DES**

A certain amount of  $\text{AgCF}_3\text{SO}_3$  was dried under the light-protected vacuum conditions at  $65^\circ\text{C}$  for 24 h, and then taken out and placed in a vacuum desiccator in a dark place. The Ag-DES was prepared by mixing DMBA and  $\text{AgCF}_3\text{SO}_3$  with a certain molar ratio of 2:1 and

then placed in a dark environment with a 60°C constant temperature oil bath for heating and stirred with an electronic digital display stirrer at 200 rpm for 1 h to form a homogeneous light yellow liquid. The synthetic route is shown in Scheme S1.

### 2.3 | Characterizations of Ag-DES

Physical property measurements mainly contain viscosity, density and thermal stability. The kinetic viscosity of the Ag-DES was tested at atmospheric pressure with the DV-III+ digital viscometer. The density of the Ag-DES was measured with the measuring cylinder and the electronic balance. Each sample was examined three times to obtain an average value under the same conditions. DTG-60AH was used for thermogravimetric analysis as a detector to place the sample on an aluminum pan under a nitrogen atmosphere. The temperature started from room temperature to a final temperature of 600°C with an increasing rate of 10°C/min. The chemical structure of Ag-DES was investigated by using FT-IR, FT-Raman, <sup>1</sup>H NMR and EIS-MS. The interaction mechanism of Ag-DES with 1-octene and n-octane was recorded by using FT-Raman spectroscopy with a 785 nm laser.

### 2.4 | Reactive extraction experiments

According to the certain concentration gradient, a series of mixtures of 1-octene and n-octane were sequentially prepared with the same weight, which were introduced into multiple 100mL flasks. Ag-DES was added into these flasks with the same volume and composition in a dark environment. The vessel was properly wrapped for the light-protection of Ag-DES to avoid quality deterioration and fixed in a thermostatic bath to maintain a constant temperature of  $T = 298.15 \pm 0.5\text{K}$ . The ternary mixtures were stirred for 1 h under the speed of 200 rpm to reach the thermodynamic equilibrium and then settled at the same temperature for 1h to get

the phase separation. The samples in organic phase were taken out by buret without disturbing the phase boundary and weighed. The reactive extraction experiments for investigating the effect of olefin concentration, molar ratio of Ag-DES to 1-octene and temperature for the ternary biphasic system were performed with the conditions shown in Table 1. Five times of circulation experiments were carried out under the same conditions, which were determined according to the TGA results for the complex of Ag-DES with 1-octene as shown in Figure S1. The complex was rotated evaporation for 12 h at a constant temperature of 65°C and depressurized at a low pressure about 1-2 kPa.<sup>29</sup> The procedure was consistent with the previous description of extraction equilibrium experiments.

**TABLE 1** The operating conditions for reactive extraction experiments on the effect of olefin concentration ( $c_1$ ), molar ratio of Ag-DES to 1-octene ( $n_{Ag}/n_1$ ), temperature ( $T$ ) and circulation stability for the ternary biphasic system

Effects	Mass of Ag-DES/g	Mass of C8/g	$c_1$ /wt.%	$n_{Ag}/n_1$	$T/^\circ\text{C}$
Olefin concentration	11.106	4.48	10/30/ 50/70/90	—	25
Molar ratio of Ag-DES to 1-octene	11.106	6.72	50	1:1/1:1.5/ 1:2/1:2.5/1:3	25
Temperature	11.106	6.72	50	1:1.5	0/10/20/ 25/30/40
Circulation stability	11.106	6.72	50	1:1.5	25

## 2.5 | GC analysis

The content of each component in the organic phase was analyzed by the PE Auto System XL Gas Chromatograph with a HP-5 non-polar chromatography column (0.32 mm × 30 m × 0.25 μm, Agilent). The content of each component in the two phases was calculated by conservation of mass as the following equations. The mass of raw material ( $M$ ) was calculated using Equation (1). Subscripts 1, 2 and 3 represent 1-octene, n-octane and Ag-DES, and superscripts org and sol represent organic phase and Ag-DES solvent phase, respectively.

$$M = m_1 + m_2 + m_3 = M^{\text{org}} + M^{\text{sol}} \quad (1)$$

where  $m_1$ ,  $m_2$  and  $m_3$  are the mass of 1-octene, n-octane and Ag-DES,  $M^{\text{org}}$  and  $M^{\text{sol}}$  stand for the total mass of organic phase and solvent phase, respectively. After the extraction equilibrium experiment, the total mass of the organic phase  $M^{\text{org}}$  and solvent phase  $M^{\text{sol}}$  can be expressed by Equations (2) and (3), respectively.

$$M^{\text{org}} = m_1^{\text{org}} + m_2^{\text{org}} + m_3^{\text{org}} \quad (2)$$

$$M^{\text{sol}} = m_1^{\text{sol}} + m_2^{\text{sol}} + m_3^{\text{sol}} = M - M^{\text{org}} \quad (3)$$

$M^{\text{org}}$  can be separated and weighed. The mass fractions of solute in the organic phase

( $x_1^{\text{org}}$ ,  $x_2^{\text{org}}$ ,  $x_3^{\text{org}} = 1 - x_1^{\text{org}} - x_2^{\text{org}}$ ) can be obtained by GC analysis and then the mass of each

component in both the two phases can be calculated by Equations (4) and (5). The content of

each component in solvent phase can be donated by Equation (6).

$$m_i^{\text{org}} = M^{\text{org}} x_i^{\text{org}}, \quad (i=1,2,3) \quad (4)$$

$$m_i^{\text{sol}} = m_i - m_i^{\text{org}}, \quad (i=1,2,3) \quad (5)$$

$$x_i^{\text{sol}} = m_i^{\text{sol}} / M^{\text{sol}}, (i=1,2,3) \quad (6)$$

## 2.6 | Simulation details

The density functional theory (DFT) quantum chemistry calculation method was employed for the analysis of Ag-DES, hydrocarbons and their complexes. All the geometric configurations were optimized by using Gaussian 09 software.<sup>30</sup> An ab initio calculation was performed with the M062X<sup>31</sup> method and def2tzvp basis set<sup>32</sup> by full optimization of energies and calculation of vibrational frequencies without any geometrical constraints. The solvent effect was considered because of its electrostatic impact on the geometries of cations and anions. There was no imaginary frequency in all of geometries and the zero-point vibrational energies (ZPEs) were also obtained for the calculation of the interaction energies between the Ag-DES and olefin/paraffin. Electron density and structural characteristics in terms of atomic components were quantitatively analyzed by multiwfn.<sup>33</sup> A series of weak interactions of intermolecular were qualitatively depicted by the isosurfaces of reduced density gradient function (RDG).<sup>34</sup> Furthermore, the covalent and strong non-covalent interactions between intermolecular were recorded and distinguished by the topological parameters at bonding critical points (BCPs) of Atoms in Molecules (AIM).<sup>35</sup>

## 3 | Ag-DES CHARACTERIZATIONS

### 3.1 | Thermal stability

TGA was conducted to examine the thermal stability of the Ag-DES. As shown in Figure 1, Ag-DES remained stable at a relatively low temperature and began to decompose until the temperature reached 160°C. An overall mass loss about 54% started at 160°C and finished at

about 330°C, which can be ascribed to the removal of DMBA. The second mass loss from 330°C to about 550°C is attributed to the decomposition process of silver trifluoromethanesulfonate. Finally, a residual mass fraction of about 20% is the involatile silver in the Ag-DES. In addition, a cooling process for stirless Ag-DES from 25°C to -20°C in 40 minutes was carried out to test its tolerance under low temperature. The fluidity gradually declined with the decreasing of temperature until loss of mobility at less than -5°C. There was a tendency to convert the solid when the temperature was further reduced after -20°C. Therefore, it can be concluded that it has a better thermal stability and a wide liquid range from -5°C to 160°C. The viscosity and density of the Ag-DES are 170.25 cP and 1.395 g/mL at room temperature, respectively.

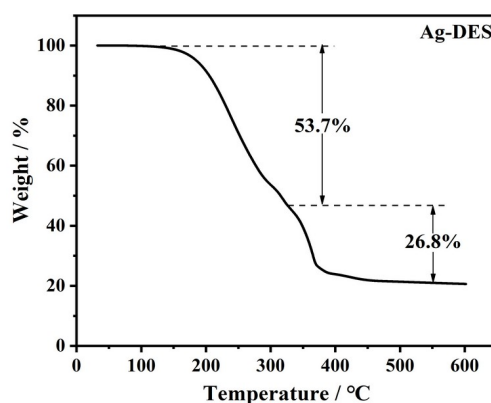
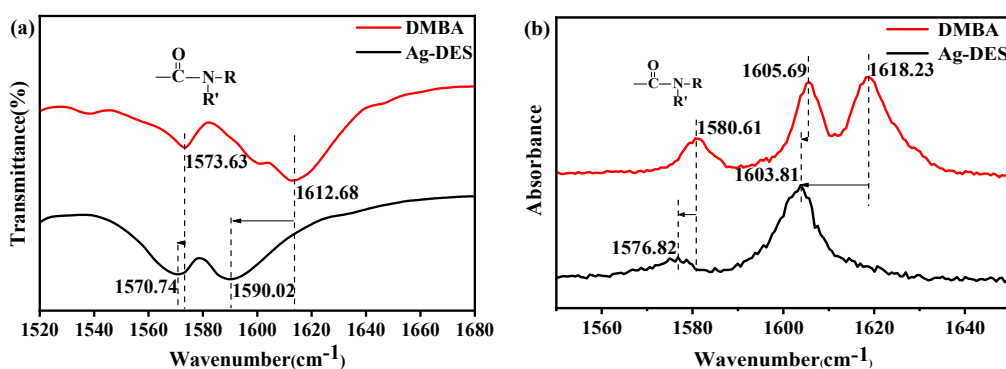


**FIGURE 1** Scanning thermal gravimetric analysis (TGA) for Ag-DES with a 10°C /min heating rate under the nitrogen atmosphere

### 3.2 | Chemical complexation in Ag-DES

The chemical complexation between silver ion and the carbon-oxygen double bond of DMBA was recorded by a series of characterization methods. The chemical structures of DMBA and Ag-DES were firstly characterized by FT-IR as shown in Figure 2(a). The peaks at 1612.68  $\text{cm}^{-1}$  and 1573.63  $\text{cm}^{-1}$  were mainly ascribed to the C=O symmetrical and

asymmetrical stretching vibration peaks in pure DMBA. After mixing with  $\text{AgCF}_3\text{SO}_3$ , both of the two peaks showed the red shifts to the position of  $1590.02\text{ cm}^{-1}$  and  $1570.74\text{ cm}^{-1}$ , respectively, which indicates that  $\text{Ag}^+$  is likely to coordinate with the O atom of the C=O donor group in Ag-DES.<sup>8</sup> Due to the low electronegativity of anion of silver salt, a strong coordination occurred between  $\text{Ag}^+$  and the O atom of C=O with higher negative charge density, which directly led to the decrease of bond energy of C=O and increase of bond length. The coordination also had the identical effect in Raman spectra as shown in Figure 2(b). The carbonyl peaks also displayed the red-shifts to the low wavenumber region, which was consistent with the FT-IR spectra. To further illustrate the above inferences, electrospray ionization mass spectrometry (ESI-MS) was performed for Ag-DES in the positive model as shown in Figure 2(c). There was a low peak at the mass-to-charge ratio ( $m/z$ ) of 108.90 for the free silver ions. Two high peaks appeared at the  $m/z$  of 256.99 and 406.08, which corresponding to the two coordination group clusters of silver ion and DMBA with the molar ratio of 1:1  $[\text{Ag}(\text{DMBA})]^+$  and 1:2  $[\text{Ag}(\text{DMBA})_2]^+$ , respectively.<sup>27</sup>



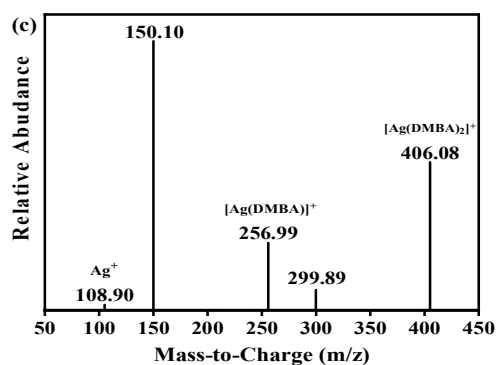
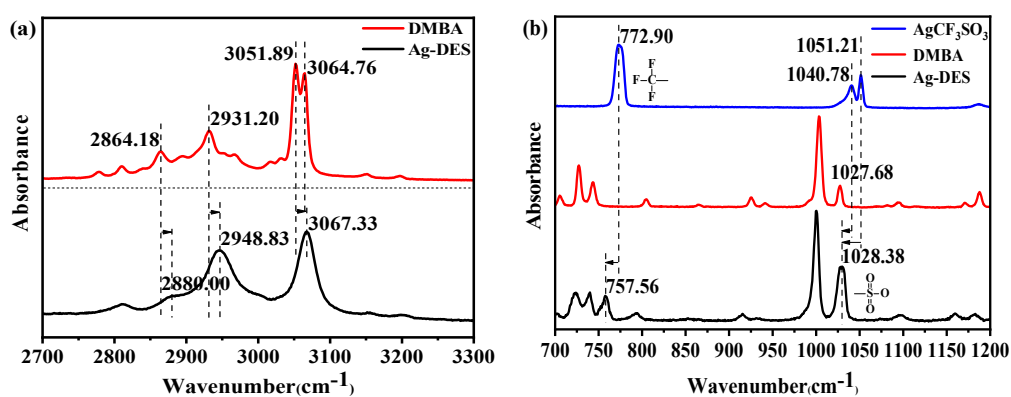


**FIGURE 2** Chemical complexation in Ag-DES recorded by FT-IR, FT-Raman and ESI-MS.

(a) FT-IR and (b) FT-Raman spectra of C=O stretching vibrations in DMBA and Ag-DES; (c) ESI-MS spectra of Ag-DES under the positive model

These results could not only illustrate the strong chemical complexation between silver ion and DMBA, but also indicate that the secondary complex is more favorable to generate than the primary complex.

### 3.3 | Hydrogen bonds in Ag-DES



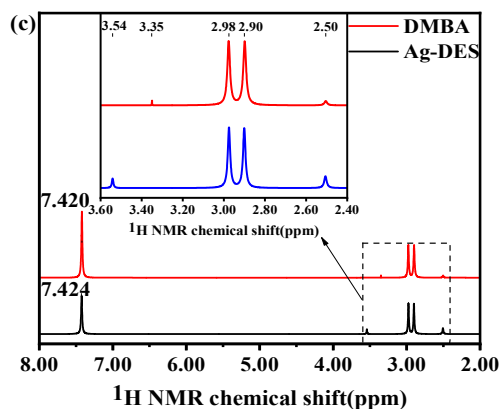


**FIGURE 3** The process of destruction and reconstruction of hydrogen bonds in Ag-DES recorded by FT-Raman and  $^1\text{H}$  NMR. (a) FT-Raman spectra of  $-\text{CH}_3$  and  $=\text{C}-\text{H}$  stretching vibrations in DMBA and Ag-DES; (b) FT-Raman spectra of  $\text{S}=\text{O}$  and  $-\text{CF}_3$  stretching vibrations in  $\text{AgCF}_3\text{SO}_3$  and Ag-DES; (c)  $^1\text{H}$  NMR spectra of DMBA and Ag-DES

Hydrogen bonds act as one of the most essential non-covalent interactions in the synthesis of deep eutectic solvent and play an important effect on the physicochemical properties.<sup>36</sup> There exists destruction and reconstruction of hydrogen bonds in the synthesis of Ag-DES as shown in Scheme S1, which can be proved by the following characterization methods as shown in Figure 3. As the FT-Raman spectra clearly shows in Figure 3(a) that the asymmetric and symmetric stretching vibration peaks of N-methyl group in DMBA at the positions of  $2864.18\text{ cm}^{-1}$  and  $2931.20\text{ cm}^{-1}$  exhibited significant blue shift to  $2880.00\text{ cm}^{-1}$  and  $2948.83\text{ cm}^{-1}$  after adding the silver triflate,<sup>37</sup> which indicates the change of chemical environment for hydrogen atoms, the hydrogen bond fracture among DMBA molecules and the formation of new stronger hydrogen bonds with higher bond energy.<sup>38,39</sup> Another pair of asymmetric and symmetric stretching vibration peaks of C-H on the benzene ring appear at  $3051.89\text{ cm}^{-1}$  and  $3064.76\text{ cm}^{-1}$  also presented a significant blue shift to  $3067.33\text{ cm}^{-1}$ .<sup>40</sup> Because the positive charge density of hydrogen atoms connected with the carbon adjacent to the substituent on

the benzene ring is higher than the others, while it is easier to form the hydrogen bonds with the oxygen and fluorine atoms from the triflate anion. In addition, the Raman spectra for  $\text{AgCF}_3\text{SO}_3$ , the hydrogen bond acceptor, is as shown in Figure 3(b). The peaks at  $1040.78\text{ cm}^{-1}$  and  $1051.21\text{ cm}^{-1}$  were mainly corresponded to the S=O asymmetrical and symmetrical stretching vibrations. However, both two peaks shifted to the low wavenumber of  $1028.38\text{ cm}^{-1}$  in Ag-DES. The red shifts caused by the elongation effect for the bond length of S=O (from  $1.430\text{ \AA}$  to  $1.448\text{ \AA}$  given by the optimized geometries) showed a decrease for the bond energy because of the reduction of negative charge density of the oxygen atoms on the sulfonic acid group to form new hydrogen bonds.<sup>37</sup> One peak at  $772.90\text{ cm}^{-1}$  was ascribed to the  $-\text{CF}_3$ , it also presented a significant red shift to  $757.56\text{ cm}^{-1}$  for the contribution of electron density to the formation of hydrogen bonds. To further illustrate the reconstruction of hydrogen bonds between the anion and DMBA, the most direct evidence for the process was carried out by  $^1\text{H}$  NMR spectra for the pure DMBA and Ag-DES as shown in Figure 3(c). The chemical shift of  $7.420\text{ ppm}$  with high intensity was related to the hydrogen on the benzene, which emerged a slight shift to the lower field of  $7.424\text{ ppm}$ , indicating that the hydrogen atoms on the benzene ring are not the primary sites for the formation of hydrogen bonds. It is obvious that a notable shift appeared at the chemical shift of  $3.35\text{ ppm}$  to  $3.54\text{ ppm}$  for the hydrogen atoms on the N-methyl group of DMBA, which actually corresponds to the hydrogen atoms for producing hydrogen bonds between DMBA molecules because the chemical shift of the other hydrogen atoms generally occurred at the range of  $2.12$  to  $3.10\text{ ppm}$ .<sup>41</sup> The coordination between the silver ion and the carbonyl oxygen atom in DMBA led to the breaking of its intermolecular hydrogen bonds. The original hydrogen atoms

with a higher positive charge density can easily form stronger hydrogen bonds with other atoms of anion, which indicates the successful synthesis of Ag-DES.

#### 4 | $\alpha$ -OLEFIN SEPARATION PERFORMANCE

In this study, Ag-DES was utilized as reactive extractant for the separation of  $\alpha$ -olefins in the 1-octene/n-octane mixture. The separation performance was evaluated by the distribution coefficient of solute  $i$  ( $D_i$ ) and the selectivity of solute  $i$  to solute  $j$  ( $S_{i,j}$ ), both of them were calculated by using Equations (7) and (8)<sup>13</sup>:

$$D_i = \frac{x_i^{sol}}{x_i^{org}}, (i = 1,2) \quad (7)$$

$$S_{i,j} = \frac{D_i}{D_j}, (i = 1, j = 2) \quad (8)$$

##### 4.1 | Effect of olefin concentration

As shown in Figure 4, the distribution coefficient of 1-octene was much greater than that of n-octane and decreased with increasing olefin concentration but n-octane slightly increased, which may be attributed to the chemical complexation between silver ion and olefin had a more significant contribution to the distribution coefficient and selectivity compared with physical dissolution effect.<sup>42</sup> Moreover, the polarity of 1-octene is greater than that of n-octane (dipole moment: 1-octene ( $\mu = 0.42$ ) > n-octane ( $\mu = 0.07$ )), which leads to the physical solubility of 1-octene is also higher than that of n-octane in the polar solvent. So the content of 1-octene in solvent phase was much greater than that of n-octane and got the higher selectivity. However, the complex sites gradually reached saturation<sup>43</sup> as the mass ratio of olefin increased and then the solubility was mainly dominated by the weak physical dissolution and the distribution coefficient of 1-octene decreased. A slight increase for n-

octane can be ascribed to the low concentration of n-octane in organic phase in the higher olefin concentration region. When the mass percent of 1-octene was as low as 10 wt.%, the selectivity could achieve 16.74, while it was as high as 90 wt.%, the selectivity only reached 3.75. Therefore, the lower olefin concentration in initio feed, the higher selectivity of 1-octene to n-octane gained.

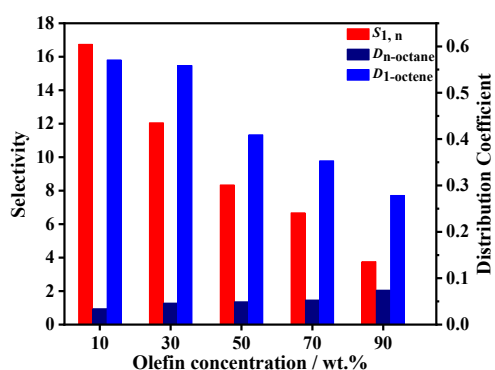


**FIGURE 4** Effect of olefin concentration on the distribution coefficient and selectivity of 1-octene to n-octane in the ternary biphasic system, including 11.106 g Ag-DES and 4.48 g C8 with the mass ratio of 1-octene in initio feed ranging from 10 wt.% to 90 wt.% at 25°C

With the reactive extraction experiments data calculated by the mass conservation shown in Table S1, the ternary phase diagram containing 1-octene + n-octane + Ag-DES was depicted as shown in Figure 5. It contains two pairs of partially miscible components and one pair of completely miscible. The solubility of 1-octene in Ag-DES is greater than that of n-octane.

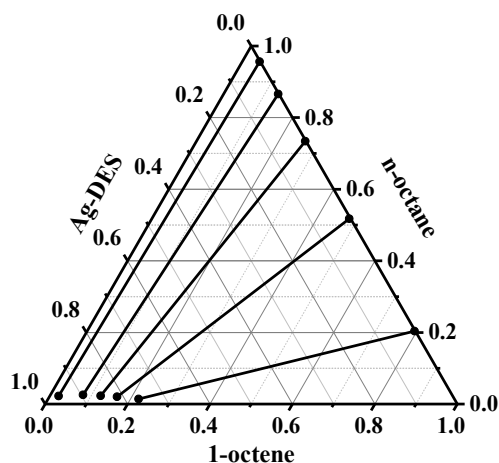


**FIGURE 5** The ternary diagram of 1-octene + n-octane + Ag-DES at  $T = 298.15 \pm 0.5\text{K}$

#### 4.2 | Effect of molar ratio of silver ion to 1-octene

As shown in Figure 6, the distribution coefficient of 1-octene raised with increasing the molar ratio of silver ion to 1-octene, which should be attributed to the more interaction sites for 1-octene with the increasing silver ion concentration.<sup>13</sup> The distribution coefficient of n-octane nearly unchanged due to the limitation of physical solubility in the Ag-DES. Furthermore, the greater the molar ratio of silver ion to olefin, the higher the selectivity of 1-octene to n-octane obtained. However, the mass fraction of 1-octene after the extraction experiment increased firstly from 1:1 to 1:2 and then decreased less than 1:2, which indicates the optimal molar ratio of silver ion to 1-octene is about 1:2. Therefore, the greater silver ion concentration is more favorable for the separation of 1-octene and n-octane and the best separation performance can be acquired at the molar ratio of 1:2.

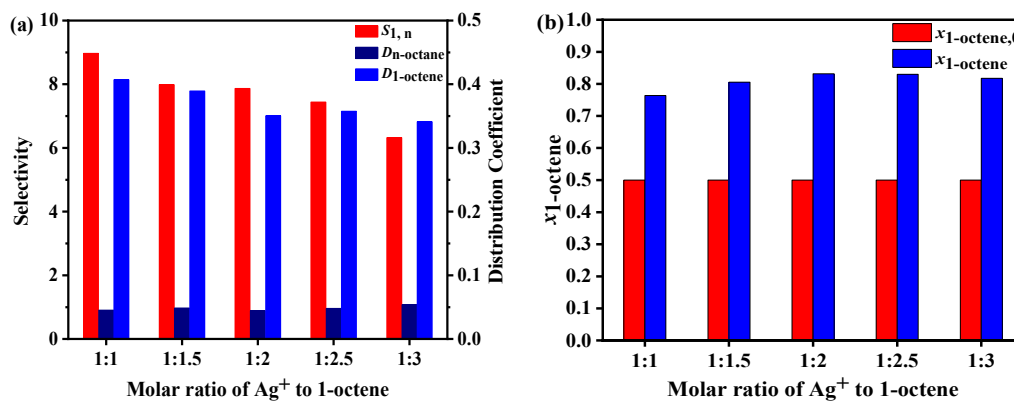


**FIGURE 6** Effect of molar ratio of silver ion to 1-octene on (a) the distribution coefficient and selectivity of 1-octene to n-octane; (b) the purification ability of 1-octene in the ternary biphasic system, including 11.106 g Ag-DES and C8 mixture with 50 wt.% olefin and the molar ratio of Ag-DES to 1-octene ranging from 1:1 to 1:3 at 25°C

#### 4.3 | Effect of temperature

The distribution coefficient of 1-octene decreased with the increasing temperature from 10°C as shown in Figure 7, which can be attributed to two reasons. On the one hand, increasing the temperature is conducive to the dissolution and diffusion of organic components in the Ag-DES.<sup>44</sup> On the other hand, increasing the temperature is negative for the chemical complexation between silver ion and olefin because the complexation is an exothermic process.<sup>45</sup> Comparing both of the two reasons, the decreased distribution coefficient of 1-octene indicates that the chemical interaction is dominant. Furthermore, the physical solubility of n-octane showed a slight increase as the temperature rises. Therefore, the selectivity of 1-octene to n-octane totally decreased with increasing temperature. However, when the operating temperature was as low as 0°C, the distribution coefficient of 1-octene and n-octane is much smaller which may be ascribed to the dominant effect of physical dissolution at such a low temperature. Consequently, the temperature with 10°C is

more favorable for the separation of 1-octene from mixture extracted by Ag-DES.

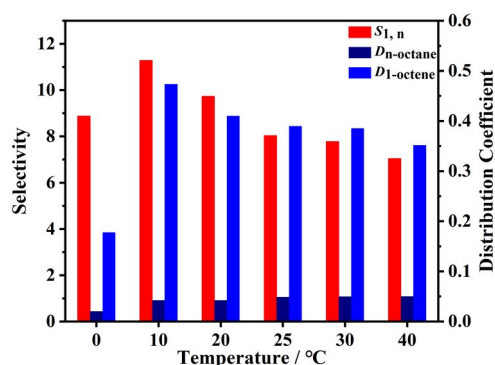


**FIGURE 7** Effect of temperature on the distribution coefficient and selectivity of 1-octene to n-octane in the ternary biphasic system, including 11.106 g Ag-DES and 6.72 g C8 mixture with 50 wt.% olefin at the temperature range of 0°C to 40°C

#### 4.4 | Circulation stability

Circulation stability is one of the most important features for an environmental solvent to apply in the separation of  $\alpha$ -olefins. As shown in Figure 8, the distribution coefficient and the selectivity of 1-octene to n-octane remained nearly unchanged, indicating that Ag-DES has a better circulation stability and repeatability for the separation of C8  $\alpha$ -olefin.

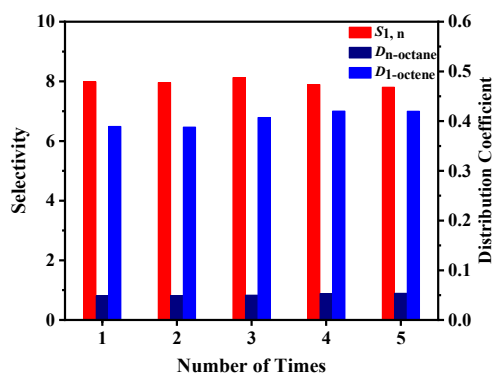


**FIGURE 8** Effect of circulation times on the distribution coefficient and selectivity of 1-octene to n-octane in the ternary biphasic system, including 11.106 g Ag-DES and 6.72 g C8 mixture with 50 wt.% olefin at 25°C for five times

#### 4.5 | The extraction performance of Ag-DES compared with ionic liquids

Compared with the past used ionic liquids, the studied Ag-DES is more favorable for the separation of 1-octene and n-octane as shown in Figure 9. The highest selectivity value 16.74 is higher than 10.74 obtained with  $[\text{Ag}(\text{DMBA})_2][\text{Tf}_2\text{N}]$  by Belluomini.<sup>14</sup> The extraction capacity value of approximately 2.48 kg Ag-DES / kg 1-octene is lower than the reported value of 5 kg  $[\text{Ag}(\text{DMBA})_2][\text{Tf}_2\text{N}]$  / kg 1-octene. Therefore, the Ag-DES shows better extraction performance than previous silver based and common ionic liquids.

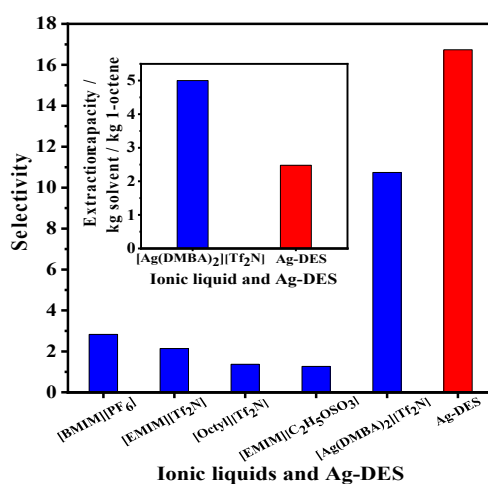


**FIGURE 9** The extraction performance of Ag-DES compared with ionic liquids. Red: Ag-DES, Blue: ionic liquids

## 5 | INTERACTION MECHANISM OF Ag-DES WITH 1-OCTENE/ N-OCTANE

### 5.1 | F-T Raman analysis

Raman analysis was performed to illustrate the interaction mechanism of Ag-DES with 1-octene and n-octane as presented in Figure 10. Comparing the spectrum of the complex with the pure components shown in Figure 10(a), it is obvious that the peak at  $1299.64 \text{ cm}^{-1}$  appeared in the purple spectrum, which indicates that 1-octene has entered the solvent Ag-

DES. If it is only caused by physical dissolution, there should exist a high peak of the carbon-carbon double bond at the position of  $1641.95\text{ cm}^{-1}$ . But the fact is that there was only a slight peak at the position of  $1640.71\text{ cm}^{-1}$  in their complex, which indicates that there was a very small amount of physical dissolution for 1-octene in the Ag-DES. In addition, the peak of the complex group of silver ion and C=O appeared at the position of  $1576.82\text{ cm}^{-1}$ , but compared with the purple spectrum after complexing 1-octene, there was a higher peak at  $1579.33\text{ cm}^{-1}$  and a slight red shift peak at  $1576.20\text{ cm}^{-1}$ .<sup>46</sup> Previous studies have reported that a new peak of the complex group of silver ion and double bond of olefin appeared at  $1585\text{ cm}^{-1}$ ,<sup>29,47</sup> it can be inferred that the new peak at  $1579.33\text{ cm}^{-1}$  should be attributed to such a new group. Because it was too close to distinguish the peak of  $1576.82\text{ cm}^{-1}$ , the total area of the peak A and peak B (The stretching vibration peak of the benzene ring at the position of  $1513.07\text{ cm}^{-1}$ ) was calculated here to confirm the chemical complexation between silver ion and olefin. In Ag-DES, the peak area ratio A/B was 0.5552, and after combining 1-octene, it obviously increased to 0.7113, which shows that a new peak of complex group overlapped and increased the area. When 1-octene was decomplexed from the complex, the A/B backed to 0.5568. Therefore, the Raman spectrum indicates the generation of chemical complexation between Ag-DES and 1-octene, which further illustrates the stability of the Ag-DES in the process of  $\alpha$ -olefins separation. Furthermore, the Raman spectrum of the complex of Ag-DES with n-octane is nearly exactly identical with that of Ag-DES as shown in Figure 10(b), the two characteristic peaks  $1304.77\text{ cm}^{-1}$  and  $1140.85\text{ cm}^{-1}$  of n-octane didn't appear in the complex spectrum, which suggests that n-octane and Ag-DES are nearly immiscible. According to the extraction experimental results, a small amount of n-octane in the Ag-DES

is attributed to the combination of 1-octene and Ag-DES because the two hydrocarbons are miscible. In summary, both of chemical complexation and stronger physical dissolution exist in the complex of Ag-DES with 1-octene, but there is almost no chemical complexation and the physical dissolution between Ag-DES and n-octane. Therefore, as an excellent DES for separation the 1-octene and n-octane, its cations should have a both strong chemical complexation and physical dissolution in order to interact strongly with the 1-octene rather than n-octane.

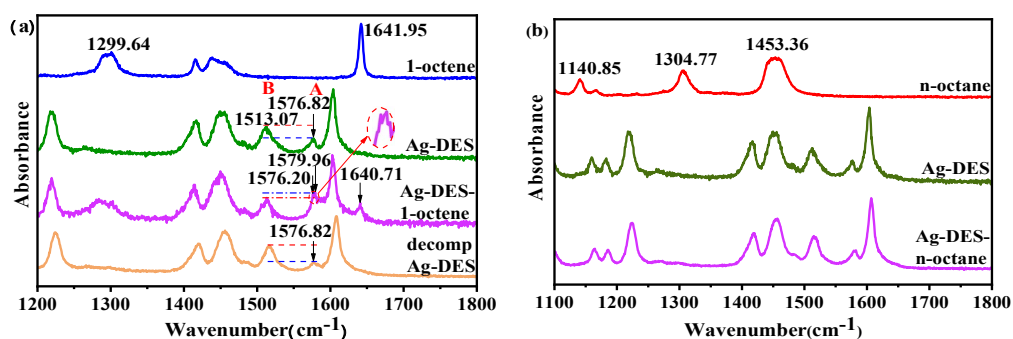


**FIGURE 10** Raman spectra of (a) Ag-DES and 1-octene and their complex at the range of 1200-1800  $\text{cm}^{-1}$ ; (b) Ag-DES and n-octane and their complex at the range of 1100-1800  $\text{cm}^{-1}$

## 5.2 | Quantum chemistry calculation

### 5.2.1 | Optimized geometries of Ag-DES and hydrocarbons

The optimized structures of 1-octene and n-octane are shown in Figure S2, the electrostatic potential (ESP) analysis of Ag-DES and its complexes with hydrocarbons are depicted in Figure S3 and their optimized structures were calculated without any imaginary frequency as displayed in Figure 11. The optimized configurations of  $\text{AgCF}_3\text{SO}_3$  and DMBA are shown in Figure 11(a) and (b). When DMBA exists alone, the carbonyl oxygen atoms and the N-methyl hydrogen atoms from two adjacent DMBA molecules can form two C-H...O hydrogen bonds

with the same H...O distance of 2.443 Å (which is shorter than the Van der Waals radius of H and O 2.72 Å<sup>48</sup>) and the C-H...O angle of 155.2°. The most stable structure for Ag-DES was optimized as displayed in Figure 11(c) after mixing AgCF<sub>3</sub>SO<sub>3</sub> and DMBA, which is consistent with the Scheme S1 that the two DMBA molecules are split on both sides by the silver salt and the two C-H...O hydrogen bonds are broken simultaneously, coordination interactions are generated between the free silver ions and the carbonyl oxygen atoms with high negative charge density. The two strong interactions C=O---Ag with the distances of 2.263 Å and 2.294 Å, the C=O---Ag angles of 102.9° and 109.5° and the O---Ag---O angle of 158.7° exist in the Ag-DES. Comparing with Figure 11(a) and (c), the distance between the silver ion and oxygen atom of the S-O increases from 2.333 Å to 2.448 Å, which suggests that the anion-cation interaction is weakened due to a part of positive charge density of silver ion is occupied by the coordination. The negative charge density of the oxygen atoms of the S=O from the anion of silver salt is higher, which can easily form C-H...O hydrogen bonds with hydrogen atoms from benzene ring (with the C-H...O distances of 2.312 Å and 2.483 Å) and N-methyl (with the C-H...O distances of 2.420 Å and 2.651 Å), etc. Therefore, both hydrogen bonds and coordination interactions exist in the synthesis process of Ag-DES, which play an important role in the stability of solvent.

The complexes of Ag-DES with 1-octene and n-octane were calculated under the SMD implicit solvent model. As displayed in Figure 11(d), a  $\pi$  bond complex is produced between silver ion and the carbon-carbon double bond of 1-octene with the C=C---Ag distances of 2.523 Å and 2.588 Å, at the same time, the C=O---Ag distances increase from original 2.263 Å and 2.294 Å to 2.342 Å and 2.429 Å, respectively, and the O---Ag---O angle increases from 158.7° to 248.9° and the C=O---Ag angles also increase from 102.9° and 109.5° to 114.1° and 118.8°, respectively, indicating that the complexation between silver ion and C=C is stronger than C=O.<sup>8</sup> Therefore the silver ion moves to the olefin, resulting in the weakness of the complexation between silver ion and carbonyl oxygen. The optimized geometry for the complex of Ag-DES and n-octane is shown in Figure 11(e), the two components are too far to form weak interactions and the structural parameters of Ag-DES remain nearly unchanged, which means that the interaction strength of 1-octene is much greater than that of n-octane.

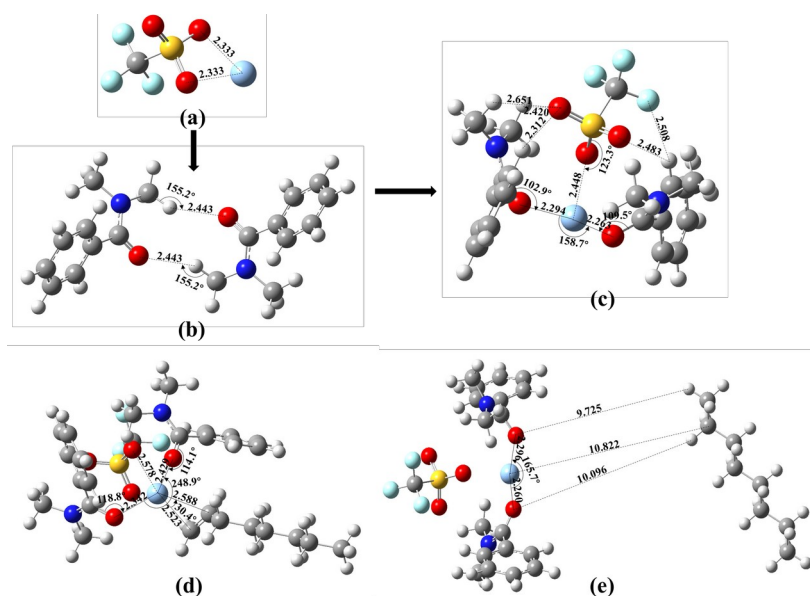


**FIGURE 11** The optimized geometry structures for (a) AgCF<sub>3</sub>SO<sub>3</sub>; (b) DMBA; (c) Ag-DES; (d) Ag-DES-1-octene; (e) Ag-DES-n-octane at the M062X/def2tzvp level

## 5.2.2 | Interaction energies analysis

Interaction energy is a physical quantity usually obtained through theoretical calculations, which can assist to describe the size of intermolecular interactions.<sup>50</sup> All geometries were optimized at the same theoretical level. The ZPEs of all components can be obtained from Gaussian view 5.0 software package.<sup>51</sup> The interaction energy of the complex AB  $E_{\text{int(AB)}}^c$  can be calculated by the following Equation (9):

$$E_{\text{int(AB)}}^c = E_{\text{(AB)}} - E_{\text{(A)}} - E_{\text{(B)}} + E_{\text{(BSSE)}} \quad (9)$$

$E_{\text{(A)}}$ ,  $E_{\text{(B)}}$  and  $E_{\text{(AB)}}$  are the ZPEs of A, B and their complex AB, respectively.  $E_{\text{(BSSE)}}$  is the energy of the basis set superposition error of A and B,<sup>52</sup> which can be calculated through the counterpoise method for more accurate interaction energies.<sup>53</sup> All results are recorded in Table 2. The interaction energy between Ag-DES and 1-octene -131.42 kJ/mol is significantly larger than n-octane -111.08 kJ/mol, and the greater difference between them will inevitably result in a stronger solubility for 1-octene in Ag-DES than n-octane.<sup>20</sup>

**TABLE 2** The interaction energies (kJ/mol) of the complexes Ag-DES(A) – 1-octene/n-octane(B) at the same M062X/def2tzvp level

Ag-DES(A)-hydrocarbon(B)	Ag-DES-1-octene	Ag-DES-n-octane
$E_{\text{A}}/(\text{kJ/mol})$	-5431268.05	-5431268.05
$E_{\text{B}}/(\text{kJ/mol})$	-825915.37	-829141.34
$E_{\text{AB}}/(\text{kJ/mol})$	-6257317.15	-6260520.47
$E_{\text{BSSE}}/(\text{kJ/mol})$	2.30	4.76E-4
$E_{\text{int(AB)}}^c/(\text{kJ/mol})$	-131.42	-111.08

### 5.2.3 | RDG analysis

Reduced Density Gradient (RDG) is a visual method for revealing weak interactions proposed by Erin R et al.<sup>34</sup> in 2010. The strength of the weak interaction is reflected by  $\rho(\tau)$  and the type needs to be judged by the  $\text{sign}(\lambda_2)$  function, which is the sign of the second largest eigenvalue  $\lambda_2$  of the electron density Hessian matrix. The  $\text{sign}(\lambda_2)$  function can be visually projected onto the RDG isosurfaces with different colors to represent the non-covalent interactions caused by electrostatic and dispersion effects for determining the physical properties existing in both intermolecular and intramolecular.

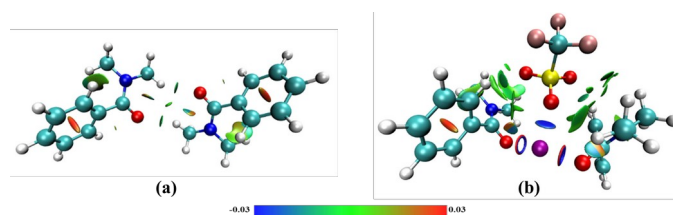


**FIGURE 12** The RDG isosurfaces for (a) DMBA; (b) Ag-DES, within the  $\text{RDG\_maxrho} = 0.05$ . The surfaces are colored on a blue - green - red (BGR) scale with the  $\text{sign}(\lambda_2)$  range from -0.03 to 0.03 au

The RDG isosurfaces are displayed in Figure 12, it can be reflected from the color scale that the interaction gradually changes from stronger attractive interactions hydrogen bonds to the weak attractive interactions Van der Waals forces, and finally shows a strong steric mutual exclusion effect. Among the two DMBA molecules depicted in Figure 12(a), there exist two cyan RDG isosurfaces representing the two C-H...O hydrogen bonds of carbonyl oxygen with N-methyl hydrogen from two DMBA molecules. After adding  $\text{AgCF}_3\text{SO}_3$ , the original

two RDG isosurfaces disappear and two deep blue hollow isosurfaces with a higher electron density exceeding  $\text{RDG\_maxrho} \ 0.05$  are formed between silver ion and the two carbonyl oxygen atoms because of the strong coordination between them as shown in Figure 12(b).<sup>8</sup> The most important is that multiple cyan and green RDG isosurfaces are generated between the hydrogen atoms from DMBA molecules and the oxygen and fluorine atoms from anion, indicating that stronger hydrogen bonds and van der Waals forces were dominated in these regions, like N-C-H...O, =C-H...O and N-C-H...F, etc. Since the type of non-covalent interactions, the number and size of the area in the visualization determine the strength of the interaction together.<sup>49</sup> It can be concluded that the hydrogen bonds between DMBA molecules breaks, forming stronger non-covalent interactions between DMBA molecules and the triflate anion in the synthesis of Ag-DES.

#### 5.2.4 | AIM analysis

The covalent interactions can usually be illustrated by atoms in molecular (AIM) theory, which can also further confirm the existence of hydrogen bonds. AIM analysis is widely employed in the determination of bond properties on the basis of topological parameters at BCPs.<sup>54</sup> The molecular graphs of Ag-DES and its complexes with 1-octene/n-octane based on AIM analysis are depicted in Figure 13. A series of topological parameters at BCPs are listed in Table S2, like the total energy density ( $H_{(\text{BCP})}$ ) to distinguish the covalent or non-covalent interactions and a bond degree parameter ( $H_{(\text{BCP})}/\rho_{(\text{BCP})}$ ) to reveal the bond strength.<sup>55</sup>

As shown in Figure 13(a), the complexation can be reflected by the BCPs of 72 and 91 between the O22-Ag9-O44 atoms in Ag-DES, which can be demonstrated by the negative

$H_{(BCP)}$  of  $-4.87E-03$  and  $-4.47E-03$ . Besides, multiple non-covalent interactions exist according to the positive  $H_{(BCP)}$ , which can be deemed to the hydrogen bonds because of the electron density  $\rho_{(r)}$  within the range of 0.002 to 0.04.<sup>56</sup> The new BCP of 148 with the negative  $H_{(BCP)}$  of  $-4.42E-03$  representing complexation between Ag9-C54=C57 atoms appears after mixing Ag-DES with 1-octene as shown in Figure 13(b). The complexation strength of Ag9-C54=C57 is stronger than that of O22-Ag9-O44 because the bond degree parameter ( $H_{(BCP)}/\rho_{(BCP)}$ ) of the former ( $-1.07E-01$ ) is more negative than that of the latter ( $-5.67E-02$  and  $-5.57E-02$ ). However, there are no any covalent interactions and hydrogen bonds existing between Ag-DES and n-octane as shown in Figure 13(c). Consequently, the AIM analysis indicates that the interaction strength of Ag-DES with 1-octene is much greater than that of n-octane, so the covalent interactions and hydrogen bonds interaction will be favorable reason for Ag-DES to interact with the double bond of 1-octene. This finding is highly consistent with experimental results, optimized geometries, and calculation of interaction energies.

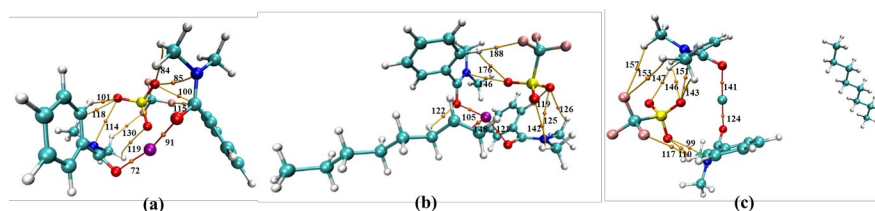


**FIGURE 13** The AIM analysis for (a) Ag-DES; (b) Ag-DES-1-octene; (c) Ag-DES-n-octane. The BCPs are marked as orange dots, the coordination covalent bonds are linked by red lines and the hydrogen bonds are linked by orange lines

## 6 | CONCLUSIONS

The first application of DESs in the separation of C8  $\alpha$ -olefin was performed with a novel silver-based deep eutectic solvent consisting of DMBA and  $AgCF_3SO_3$ . Its structure was well

characterized by FT-IR, FT-Raman, ESI-MS and  $^1\text{H}$  NMR, which illustrated the successful preparation of Ag-DES. The separation performance in C8  $\alpha$ -olefin was carried out and showed that the lower olefin concentration and higher silver ion concentration, the larger the selectivity of 1-octene to n-octane obtained. The Ag-DES possessed better performance in the separation of 1-octene/n-octane than those ionic liquids in previous studies, the selectivity could even reach 16.74 for 1-octene to n-octane with the olefin concentration of 10 wt.% in the initial feed at 298.15K. An increase in temperature decreased the selectivity and distribution coefficient for 1-octene because the effect of chemical complexation on selectivity is more significant than physical dissolution. Furthermore, the Ag-DES exhibited an excellent circulation stability, which has great application potential for the separation of long chain  $\alpha$ -olefins. In addition, FT-Raman and quantum chemistry calculation were investigated for the determination of interaction between Ag-DES and 1-octene/n-octane. Raman spectra, optimized geometries, interaction energies and AIM topological analysis showed that both the physical dissolution and chemical complexation exist in the complex of Ag-DES with 1-octene, but there is nearly no weak interaction between Ag-DES and n-octane. Therefore, the great interaction difference of Ag-DES with 1-octene and n-octane achieved the excellent separation performance for 1-octene/n-octane.

#### **ACKNOWLEDGMENTS**

The authors are grateful for the financial support from the National Key R&D Program of China (2018YFB0604900), as well as Key Research and Development program of Ningxia (2018BDE02057).

## REFERENCES

1. Yang RH, Gao RM, Qian Z, Wang YJ. Batch and fixed bed column selective adsorption of C-6, C-8 and C-10 linear alpha-olefins from binary liquid olefin/paraffin mixtures onto 5A and 13X microporous molecular sieves. *Sep Purif Technol.* 2020;230:115884.
2. Wentink AE, Kuipers NJM, de Haan AB, Scholtz J, Mulder H. Olefin isomer separation by reactive extractive distillation: Modelling of vapour-liquid equilibria and conceptual design for 1-hexene purification. *Chem Eng Process-Process Intensif.* 2007;46(9):800-809.
3. Kuipers NJM, Wentink AE, de Haan AB, Scholtz J, Mulder H. Functionalized solvents for olefin isomer purification by reactive extractive distillation. *Chem Eng Res Des.* 2007;85(A1):88-99.
4. Eagan NM, Moore BM, McClelland DJ, et al. Catalytic synthesis of distillate-range ethers and olefins from ethanol through Guerbet coupling and etherification. *Green Chem.* 2019;21(12):3300-3318.
5. Sun H, Ren DN, Kong RQ, et al. Tuning 1-hexene/n-hexane adsorption on MOF-74 via constructing Co-Mg bimetallic frameworks. *Micropor Mesopor Mat.* 2019;284:151-160.
6. Piszczek R, Heins B, Hamilton P, et al. Separating linear alpha olefin involves providing a pre-processed product stream comprising linear alpha olefins to first of series of distillation columns, and element of the series of distillation columns comprising a dividing wall column, WO2020114744-A1; 2020.
7. Yang R, Gao R, Wang Y, Qian Z, Luo G. Selective Adsorption of C6, C8, and C10

- Linear alpha-Olefins from Binary Liquid-Phase Olefin/Paraffin Mixtures Using Zeolite Adsorbents: Experiment and Simulations. *Langmuir*. 2020;36(29):8597-8609.
8. Fallanza M, Ortiz A, Gorri D, Ortiz I. Experimental study of the separation of propane/propylene mixtures by supported ionic liquid membranes containing Ag<sup>+</sup>-RTILs as carrier. *Sep Purif Technol*. 2012;97:83-89.
  9. Chen J, Eldridge RB, Rosen EL, Bielawski CW. A Study of Cu(I)- Ethylene Complexation for Olefin-Paraffin Separation. *AIChE J*. 2011;57(3):630-644.
  10. Safarik DJ, Eldridge RB. Olefin/paraffin separations by reactive absorption: A review. *Ind Eng Chem Res*. 1998;37(7):2571-2581.
  11. Liu Z, Zhang LY, Li LF, Zhang SY. Separation of olefin/paraffin by electrodialysis. *Sep Purif Technol*. 2019;218:20-24.
  12. Rychlewska K, Kujawski W, Konieczny K. Pervaporative performance of PEBA and PDMS based commercial membranes in thiophene removal from its binary mixtures with hydrocarbons. *Fuel Process Technol*. 2017;165:9-18.
  13. Li R, Xing H, Yang Q, et al. Selective Extraction of 1-Hexene Against n-Hexane in Ionic Liquids with or without Silver Salt. *Ind Eng Chem Res*. 2012;51(25):8588-8597.
  14. Belluomini GJ, Pendergast JG, Domke CH, Ussing BR. Performance of Several Ionic Liquids for the Separation of 1-Octene from n-Octane. *Ind Eng Chem Res*. 2009;48(24):11168-11174.
  15. Dou HZ, Jiang B, Xu M, Zhou JH, Sun YL, Zhang LH. Supported ionic liquid membranes with high carrier efficiency via strong hydrogen-bond basicity for the sustainable and effective olefin/paraffin separation. *Chem Eng Sci*. 2019;193:27-37.
  16. Zhang QH, Vigier KD, Royer S, Jerome F. Deep eutectic solvents: syntheses,

- properties and applications. *Chem Soc Rev.* 2012;41(21):7108-7146.
17. Smith EL, Abbott AP, Ryder KS. Deep Eutectic Solvents (DESS) and Their Applications. *Chem Rev.* 2014;114(21):11060-11082.
  18. Esfahani HS, Khoshsima A, Pazuki G. Choline chloride-based deep eutectic solvents as green extractant for the efficient extraction of 1-butanol or 2-butanol from azeotropic n-heptane + butanol mixtures. *J Mol Liq.* 2020;313:113524.
  19. Dai YT, van Spronsen J, Witkamp GJ, Verpoorte R, Choi YH. Ionic Liquids and Deep Eutectic Solvents in Natural Products Research: Mixtures of Solids as Extraction Solvents. *J Nat Prod.* 2013;76(11):2162-2173.
  20. Liu FJ, Chen W, Mi JX, et al. Thermodynamic and molecular insights into the absorption of H<sub>2</sub>S, CO<sub>2</sub>, and CH<sub>4</sub> in choline chloride plus urea mixtures. *AIChE J.* 2019;65(5):e16574.
  21. Cao YK, Zhang XP, Zeng SJ, Liu YR, Dong HF, Deng C. Protic ionic liquid-based deep eutectic solvents with multiple hydrogen bonding sites for efficient absorption of NH<sub>3</sub>. *AIChE J.* 2020;66(8):e16253.
  22. Faisal M, Haider A, ul Aein Q, Saeed A, Larik FA. Deep eutectic ionic liquids based on DABCO-derived quaternary ammonium salts: A promising reaction medium in gaining access to terpyridines. *Front Chem Sci Eng.* 2019;13(3):586-598.
  23. Qin H, Song Z, Zeng Q, Cheng HY, Chen LF, Qi ZW. Bifunctional imidazole-PTSA deep eutectic solvent for synthesizing long-chain ester IBIBE in reactive extraction. *AIChE J.* 2019;65(2):675-683.
  24. Li G, Row KH. Utilization of deep eutectic solvents in dispersive liquid-liquid micro-extraction. *Trac-Trends Anal Chem.* 2019;120:115651.

25. Ren XY, Zhu XL, Xu CY, et al. The Electrodeposition of Amorphous/Nanocrystalline Ni-Cr Alloys from ChCl-EG Deep Eutectic Solvent. *J Electrochem Soc.* 2020;167(6):062502.
26. Wadekar PH, Khose RV, Pethsangave DA, Some S. One-Pot Synthesis of Sulfur and Nitrogen Co-Functionalized Graphene Material using Deep Eutectic Solvents for Supercapacitors. *Chemsuschem.* 2019;12(14):3326-3335.
27. Jiang B, Dou HZ, Wang BY, et al. Silver-Based Deep Eutectic Solvents as Separation Media: Supported Liquid Membranes for Facilitated Olefin Transport. *Acs Sustain Chem Eng.* 2017;5(8):6873-6882.
28. Sun YL, Bi HR, Dou HZ, et al. A Novel Copper(I)-Based Supported Ionic Liquid Membrane with High Permeability for Ethylene/Ethane Separation. *Ind Eng Chem Res.* 2017;56(3):741-749.
29. Wang Y, Thompson J, Zhou JJ, et al. Use of water in aiding olefin/paraffin (liquid plus liquid) extraction via complexation with a silver bis(trifluoromethylsulfonyl)imide salt. *J Chem Thermodyn.* 2014;77:230-240.
30. Frisch MJ, Trucks GW, Schlegel HB, et al. *Gaussian 09*, Revision C. 01. Gaussian, Inc., Wallingford, CT. 2010.
31. Zhao Y, Truhlar DG. The M06 suite of density functionals for main group thermochemistry, thermochemical kinetics, noncovalent interactions, excited states, and transition elements: two new functionals and systematic testing of four M06-class functionals and 12 other functionals. *Theor Chem Acc.* 2008;120(1-3):215-241.
32. Weigend F, Ahlrichs R. Balanced basis sets of split valence, triple zeta valence and quadruple zeta valence quality for H to Rn: Design and assessment of accuracy. *Phys*

*Chem Chem Phys.* 2005;7(18):3297-3305.

33. Tian L. Multiwfn: a multifunctional wavefunction analyzer. *J comput chem.* 2012;5(33).
34. Erin R J. Revealing noncovalent interactions. *J Am Chem Soc.* 2010;18(132):6498-6506.
35. Bader RFW. Atoms in molecules. *Acc Chem Res.* 1985;18(1):9-15.
36. Dalvit C, Vulpetti A. Weak Intermolecular Hydrogen Bonds with Fluorine: Detection and Implications for Enzymatic/Chemical Reactions, Chemical Properties, and Ligand/Protein Fluorine NMR Screening. *Chem-Eur J.* 2016;22(22):7592-7601.
37. Alabugin IV, Manoharan M, Peabody S, Weinhold F. Electronic Basis of Improper Hydrogen Bonding: A Subtle Balance of Hyperconjugation and Rehybridization. *J Am Chem Soc.* 2003;125(19):5973-5987.
38. Trivedi TJ, Lee JH, Lee HJ, Jeong YK, Choi JW. Deep eutectic solvents as attractive media for CO<sub>2</sub> capture. *Green Chem.* 2016;18(9):2834-2842.
39. Pan-Pan Z, Wen-Yuan Q. Red- and blue-shifted hydrogen bonds in the cis-trans noncyclic formic acid dimer. *Chemphyschem.* 2009;10(11):1847-1858.
40. Eren B, Unal A. Molecular structure and spectroscopic analysis of 1,4-Bis(1-methyl-2-benzimidazolyl)benzene; XRD, FT-IR, dispersive-Raman, NMR and DFT studies. *Spectrochim Acta A.* 2013;103:222-231.
41. Hao CX, Zhao L, Yue XQ, Pang YJ, Zhang JB. Density, dynamic viscosity, excess properties and intermolecular interaction of triethylene glycol plus N,N-dimethylformamide binary mixture. *J Mol Liq.* 2019;274:730-739.
42. Ahosseini A, Sensenich B, Weatherley LR, Scurto AM. Phase Equilibrium,

- Volumetric, and Interfacial Properties of the Ionic Liquid, 1-Hexyl-3-methylimidazolium Bis(trifluoromethylsulfonyl)amide and 1-Octene. *J Chem Eng Data*. 2010;55(4):1611-1617.
43. Wentink AE, Kockmann D, Kuipers NJM, de Haan AB, Scholtz J, Mulder H. Effect of C6-olefin isomers on pi-complexation for purification of 1-hexene by reactive extractive distillation. *Sep Purif Technol*. 2005;43(2):149-162.
  44. Jiang B, Dou HZ, Zhang LH, et al. Novel supported liquid membranes based on deep eutectic solvents for olefin-paraffin separation via facilitated transport. *J Memb Sci*. 2017;536:123-132.
  45. Ortiz A, Galan LM, Gorri D, de Haan AB, Ortiz I. Reactive Ionic Liquid Media for the Separation of Propylene/Propane Gaseous Mixtures. *Ind Eng Chem Res*. 2010;49(16):7227-7233.
  46. Jung KW, Kang SW. Effect of functional group ratio in PEBAX copolymer on propylene/propane separation for facilitated olefin transport membranes. *Sci Rep*. 2019;9:11454.
  47. Sunderrajan S, Freeman BD, Hall CK. Fourier transform infrared spectroscopic characterization of olefin complexation by silver salts in solution. *Ind Eng Chem Res*. 1999;38(10):4051-4059.
  48. Bondi A. van der Waals Volumes and Radii. *J Phys Chem A*. 1964;68(3):441-451.
  49. Li H, Zhou P, Zhang J, Li DY, Li XG, Gao X. A theoretical guide for screening ionic liquid extractants applied in the separation of a binary alcohol-ester azeotrope through a DFT method. *J Mol Liq*. 2018;251:51-60.
  50. Okoshi M, Yamada Y, Komaba S, Yamada A, Nakai H. Theoretical Analysis of

- Interactions between Potassium Ions and Organic Electrolyte Solvents: A Comparison with Lithium, Sodium, and Magnesium Ions. *J Electrochem Soc.* 2017;164(2):A54-A60.
51. Dennington RD, Keith TA, Millam JM. *GaussView 5*. Gaussian, Inc., Wallingford, CT. 2009.
  52. Handy NC. The calculation of small molecular interactions by the differences of separate total energies. Some procedures with reduced errors. *Molecular Physics*. 2002;100(1):63-63.
  53. Boys SF, Bernardi F. The calculation of small molecular interactions by the differences of separate total energies. Some procedures with reduced errors (Reprinted from *Molecular Physics*, vol 19, pg 553-566, 1970). *Mol Phys*. 2002;100(1):65-73.
  54. Cao BB, Du JY, Cao ZP, Sun HT, Sun XJ, Fu H. Theoretical study on the alkylation of o-xylene with styrene in AlCl<sub>3</sub>-ionic liquid catalytic system. *J Mol Graph Model*. 2017;74:8-15.
  55. Cremer D, Kraka E. Chemical Bonds without Bonding Electron Density — Does the Difference Electron-Density Analysis Suffice for a Description of the Chemical Bond? *Angew. Chem. Int. Ed. Engl.* 1984;23(8):627-628.
  56. Lipkowski P, Grabowski SJ, Robinson TL, Leszczynski J. Properties of the C-H center dot center dot center dot H dihydrogen bond: An ab initio and topological analysis. *J Phys Chem A*. 2004;108(49):10865-10872.

## SUPPORTING INFORMATION

Tables of liquid-liquid phase equilibrium experimental data, some other topological parameters of BCPs involved in this work. Figures for part of optimized structures of

hydrocarbons and TGA results for complex.